Activity trends of binary silver alloy nanocatalysts for oxygen reduction reaction in alkaline media

Wu, Xiaoqiang; Chen, Fuyi; Zhang, Nan; Lei, Yimin; Jin, Yachao; Qaseem, Adnan; Johnston, Roy L.

DOI:
10.1002/smll.201603387

Document Version
Peer reviewed version

Citation for published version (Harvard):
Wu, X, Chen, F, Zhang, N, Lei, Y, Jin, Y, Qaseem, A & Johnston, RL 2017, 'Activity trends of binary silver alloy nanocatalysts for oxygen reduction reaction in alkaline media', *Small*, vol. 13, no. 15, 1603387. https://doi.org/10.1002/smll.201603387

WILEY-VCH

DOI: 10.1002/ ((please add manuscript number))

Article type: Full Paper

Activity Trends of Binary Silver Alloy Nanocatalysts for Oxygen Reduction Reaction in Alkaline Media

Xiaoqiang Wu,[a] Fuyi Chen,[a] Nan Zhang,[a] Yimin Lei,[a] Yachao Jin,[a] Adnan Qaseem,[a] and Roy L. Johnston[b]*

X.Q. Wu, F.Y. Chen, N. Zhang, Y.M. Lei, Y.H. Jin, A. Qaseem,
State Key Laboratory of Solidification Processing, Northwestern Polytechnical University, Xian, 710072, China
E-mail: fuyichen@nwpu.edu.cn (Fuyi Chen)

Roy L. Johnston
Department of Chemistry, University of Birmingham, Birmingham, B15 2TT, U.K.

Key words: Ag-based alloy; oxygen reduction; electronic structure; d-band centre; electrocatalysts

Abstract: The electrocatalytic activity of Pt-based alloys exhibits a strongly dependence on their electronic structures, but a relationship between electronic structure and oxygen reduction reaction (ORR) activity in Ag-based alloys is still not clear. Here, a vapor deposition based approach is reported for the preparation of $Ag_{75}M_{25}$ (M=Cu, Co, Fe and In) and Ag_xCu_{100-x} (x=0, 25, 45, 50, 55, 75, 90 and 100) nanocatalysts and their electronic structures are determined by valence band spectra. The relationship of the d-band centre and ORR activity exhibits volcanno-shape behaviors, where the maximum catalytic activity obtained for $Ag_{75}Cu_{25}$ alloys. The ORR enhancement of $Ag_{75}Cu_{25}$ alloys originates from the 0.12eV upshift in d-band center relative to pure Ag, which is different from the downshift in the d-band center in Pt-based alloys. The activity trend for these $Ag_{75}M_{25}$ alloys is in the order

of $Ag_{75}Cu_{25}$> $Ag_{75}Fe_{25}$> $Ag_{75}Co_{25}$. These results provide an insight to understand the activity and stability enhancement of $Ag_{75}Cu_{25}$ and $Ag_{50}Cu_{50}$ catalysts by alloying.

1.Introduction

The oxygen reduction reaction (ORR) is critical for alkaline fuel cells and metal-air batteries, Pt and Pt-based alloys are known as the most efficient catalysts for ORR, however, their cost and scarcity in the earth crust have hampered their extensive application.[1] To make ORR catalysts more economical and viable, there are many problems that should be solved. The main one is to find a low cost and highly active catalyst to substitute Pt. Silver has been known as an inexpensive catalyst which could achieve this goal because of its acceptable catalytic activity, high stability in alkaline solution and low cost (about 50 times less expensive than Pt).[2] However, the rational screening of inexpensive, stable and efficient Ag-based electrocatalysts requires the understanding of the catalysis mechanisms, catalytic behavior and intrinsic effect (such as electronic effect) of these catalysts in ORR process.[3]

Recently, our group reported that the electronic perturbation to play a key role on activity and stability of Ag-Cu metallic glass electrocatalysts with performance comparable to Pt/C for zinc–air batteries.[4] Similarly Nørskov *et al.* identified the electronic effect as a factor which determined the ORR activity order of Pt-based alloys and provided a basis for the future optimal design of active and stable Pt-based catalysts.[5] But to the best of our knowledge, the ORR activity order has been rarely reported for Ag-based alloys. To this end, in 2014, Holewinski et al. reported the Ag-Co alloy had an excellent ORR performance, where the subsurface Co atoms provided the electronic perturbation or ligand effect, reaching up to almost half ORR activity of Pt at 0.8 V_{RHE} in alkaline media.[6] From the theoretical calculations on the Ag-Co near surface alloy (NSA), the free energy diagram for ORR on the (111) surface of binary $Ag_{75}M_{25}$ (M=Cu, Co and Fe) alloys were studied and a activity order is obtained as Pt > Ag-Fe >Ag-Co >Ag-Cu >Ag. Nevertheless, this theoretical activity order

is still short of the direct experimental support and is not considering the contribution of other surface, such as, the (311), (200)/(100) and (220)/(110) facets, which are suggested to be more suitable for ORR in Ag-based and Pt-based alloys.[7] Yi et al. reported the activity order of binary silver-based nanocatalysts supported on carbon nanotube (CNT) for ORR in alkaline media,[8] it is reported that the activity of Ag-based alloys is in order of Ag_8Co_2/CNT > Ag_9Cu_1/CNT > Ag/CNT, and the activity of Ag_9Cu_1/CNT is severely deteriorated after a single polarization test on rotating disk electrode at 1600 rpm, suggesting a very low ORR stability. On the contrary, the theoretical calculations from Kim et al. [3b, 9] and our group[10] reported that Ag-Cu alloy nanocatalysts posses higher ORR activity and stability than pure Ag. Our recent experimental work also shows that Ag-Cu alloy catalyst has good activity and stability for ORR in alkaline media and presents excellent cyclic performance during charging-discharging in real zinc–air batteries. [11] It is well-known that CNTs are active for ORR in alkaline media, so the activity order of Ag-based alloys supported on CNT is not a realistic portrayal of the alloying effect in Ag catalyst.[12] It can be inferred that the present ORR activity order obtained from the (111) facets of Ag-M alloys [6] or from CNT-supported Ag-M alloys [8] may be different with the real Ag-based alloys.

Herein, we directly deposited the $Ag_{75}M_{25}$ (M=Cu, Co, In and Fe) and Ag_xCu_{100-x} (x= 0, 25, 45, 50, 55, 75, 90 and 100) alloys on glassy carbon electrode via pulsed laser deposition (PLD) and measured their activity order via rotating disk electrode (RDE) polarization test. As a function of electronic perturbation in ORR, a volcano curve (specific activity vs. d-band center) for Ag-based catalysts was built and a activity order of these alloys was obtained. This volcano curve provides guidance for the screening of Ag alloy catalysts, explains the enhancement effects from the electronic perturbation, and provides new insight into the design of alkaline fuel cells and metal-air batteries.

2. Results and discussion

2.1. The ORR activity of the $Ag_{75}M_{25}$ and Ag_xCu_{100-x} alloys

Figure 1a and **Figure S2** show the RDE polarization curves of $Ag_{75}M_{25}$ alloys measured in an O_2-saturated 0.1 M KOH, **Table 1** list their ORR activities. The $Ag_{75}M_{25}$ alloys demonstrate their catalytic activity changes via alloying Ag with the M elements, the half-potentials are in the order as:Pt/C-20% ($0.88V_{RHE}$) >$Ag_{75}Cu_{25}$ ($0.76V_{RHE}$) >$Ag_{75}Fe_{25}$ ($0.73V_{RHE}$)> $Ag_{75}Co_{25}$ ($0.70V_{RHE}$) > Ag ($0.66V_{RHE}$)>$Ag_{75}In_{25}$ ($0.56V_{RHE}$), indicatind that the ORR activity of Ag is significantly changed by alloying with M (M=Co, Fe and Cu) metals. Further more, we consider the effect of amount of alloying element by carrying out activity measurements for different amount of Cu in Ag_xCu_{100-x} alloys (see **Figure 1a, Figure S3** and **Table 1**). By tuning the composition of Cu, the half-wave potential of Ag_xCu_{100-x} alloys showed a pattern of normal distribution, indicating the ORR activity is tuned by content of Cu. However, if the content of Cu become extremly high, the half-wawe potential decreases because the excessive Cu atoms would occupy the position of Ag and decreases the activity site. In Cu contents ranging 0 to 50 at%, the activity of Ag_xCu_{100-x} alloys is improved with increasing of Cu content, alloying effect play a positive role. In the Cu contents higher than 50%, the activity of Ag_xCu_{100-x} alloys is decreased with increasing of Cu content.

The corresponding Koutecky-Levich (K-L) plots at $0.3V_{RHE}$ electrode potential shown in **Figure S4** are used to evaluate the transferred electron number per oxygen molecule in ORR. The K-L plots for Ag_xCu_{100-x} and $Ag_{75}M_{25}$ catalysts display good linearity. The n values for $Ag_{75}M_{25}$ (M=Cu, Co and Fe) catalysts as calculated by K-L equations at 0.30 V_{RHE} is 3.86, 3.82 and 3.84 respectively, demonstrating an apparent quasi-four-electron process in the $Ag_{75}M_{25}$ catalyst.[13] For Ag_xCu_{100-x} (x=0, 25, 45, 50, 55, 75, 90 and 100) alloys, the highest electron transfer number value at 0.30 V_{RHE} is 3.97 for x=50, indicating that $Ag_{50}Cu_{50}$ alloy catalysts favor four-electron reduction process.

To further determine the acitivity order of $Ag_{75}M_{25}$ and Ag_xCu_{100-x} alloys, we considered the specific activity and Tafel slopes of them. **Figure 1b** shows that the

corresponding specific activity (SA) and mass specific activity (MA) curves of these alloys in ORR polarization test at 0.85V_{RHE}. Both SA and MA results indicate that the $Ag_{75}Cu_{25}$ alloy (0.85 mA cm^{-2} and 89.5 A g_{total}^{-1}) is the most ORR active alloy among $Ag_{75}M_{25}$ alloys, and $Ag_{50}Cu_{50}$ alloy (1.57 mA cm^{-2} and 207.5 A g_{total}^{-1}) is the most ORR active composition among Ag_xCu_{100-x} alloys. For refining these results, we considered the corresponding electrochemical surface areas (ECSA) of these $Ag_{75}M_{25}$ and Ag_xCu_{100-x} alloys as present in **Figure 1c, Figure S5** and **Table 1**. The ECSA of pure Ag (14.05 m^2 g_{total}^{-1}) is lower than that of Ag-M alloys (range from 15.22 g_{total}^{-1} to 16.49 g_{total}^{-1}), suggesting a lower specific surface area of Ag catalyst(see **Table S1**). But for Ag-M alloys, the ECSA is almost the same. This result is in agreement with the TEM results (support information in Part 4), in which the pure Ag nanoparticles are bigger than that of Ag-M alloys and results a lower ECSA. Using the polarization curves of **Figure 1a**, the Tafel slopes (*K*) were observed for ORR on these Ag_xCu_{100-x} and $Ag_{75}M_{25}$ alloys. As shown in **Figure 1d and Table 1**, after alloying with other metals, the Tafel slopes in the low overpotential range is in the order of $Ag_{75}Cu_{25}$(72 mV dec^{-1}) < $Ag_{75}Fe_{25}$(76mV dec^{-1})< $Ag_{75}Co_{25}$(78 mV dec^{-1})< $Ag_{75}In_{25}$(81mV dec^{-1}). This result is in concomitant with the orders of specific activity and mass activity. For Ag_xCu_{100-x} alloys, the Tafel slope in the low overpotential range increases with the increasing of Cu content (range from 0 to 50%) as Ag (79 mV dec^{-1}) < $Ag_{90}Cu_{10}$ (78 mV dec^{-1}) < $Ag_{75}Cu_{25}$ (72 mV dec^{-1}) < $Ag_{55}Cu_{45}$ (69 mV dec^{-1}). When the Cu content is higher than 50%, the Tafel slopes increase with the increasing of Cu-content as $Ag_{50}Cu_{50}$ (64 mV dec^{-1}) < $Ag_{45}Cu_{55}$ (66 mV dec^{-1}) < $Ag_{25}Cu_{75}$ (75 mV dec^{-1}). Here, the $Ag_{50}Cu_{50}$ exhibits smallest Tafel slope and is therefore the most efficient ORR catalyst among all the catalysts in this study, suggesting an outstanding intrinsic ORR kinetics of $Ag_{50}Cu_{50}$ alloy. Meanwhile, the better ORR catalytic activity of $Ag_{50}Cu_{50}$ alloy compared to other Ag_xCu_{100-x} (x= 25, 45, 55, 75, 90) alloys catalysts demonstrated that the content of Cu plays an important role in determining the ORR pathway.

2.2. The d-band center of the $Ag_{75}M_{25}$ and Ag_xCu_{100-x} alloys

As mentioned above, the alloying of Ag with M (Co, Fe, Cu and In) significantly changes the catalytic activity of Ag, the question arises as to why the catalytic property can be tuned by chemical composition. Considering that Pt-based alloys employe the d-band center to address this question and the role of electronic perturbation has been justified[5], the valence band spectra (VBS) of various $Ag_{75}M_{25}$ alloys were measured by high-resolution X-ray photoelectron spectroscopy (XPS). **Figure 2a** show the VBS spectra of the pure Ag and $Ag_{75}M_{25}$ alloys, and **Table 2** listed the d-band center of VBS. It is shown that the surface electronic structure of $Ag_{75}M_{25}$ alloys is different from that of pure Ag, which posses a innate d-band center at -5.28eV. This d-band center of Ag coincides with the results of Timo Hofmann et al.[3a] Careful inspection of the VBS in **Figure 2a** reveals that the density of states (DOS) of $Ag_{75}M_{25}$ (Co, Fe and Cu) alloys present a clearly discernible increase near the Fermi level, that is, the position of d-band center is upshifted relative to pure Ag. But for $Ag_{75}In_{25}$, the DOS is increased in the far end of VBS which leads to a downshift of d-band center to -5.51eV. Hence, the M (Cu, Co, Fe and In) elements modulate the electronic structure and affect ORR activity of Ag in $Ag_{75}M_{25}$ alloys.

To obtain the further insight of the d-band center of $Ag_{75}M_{25}$ alloys, the density functional theory (DFT) calculations are performed on pure Ag, $Ag_{75}Cu_{25}$, $Ag_{75}Co_{25}$, $Ag_{75}Fe_{25}$ and $Ag_{75}In_{25}$ (Details of model and calculation methods are shown in the Supporting Information.). As present in **Figure S6** and **Table S2**, after alloying with the M with the exception of In element, the densty of state (DOS) near Fermi level of $Ag_{75}M_{25}$ alloys, between 1eV and 2.5eV, present a clearly discernible increase with addition of Cu, Fe and Cu elements. The change of the d-band centers is in the order as: AgIn(-4.65eV) <Ag(-4.61eV) <AgCu(-4.51eV) <AgFe(-4.41eV) <AgCo(-4.34eV). Although the calculated d-band center from DFT is different from the experimetal d-band centers from VBS, the trends of d-band center change and the increasing of DOS near fermi level between 0 and -2.5 eV are coincide

with the experimetal XPS results in **Figure 2a and 2c,** demonstrating the electronic perturbation plays a critical role on the d-band center of the $Ag_{75}M_{25}$ alloys.

As shown in **Figure 1a**, the ORR activity of Ag_xCu_{100-x} alloys depend on the Cu content. To explore the overall consequence of both the alloying element M and the content of M with the aim to create a more efficient catalyst than pure Ag, we considered the effects of Cu content on VBS of the Ag_xCu_{100-x} alloys. **Figure 2b** present the VBS spectra of the pure Ag and Ag_xCu_{100-x} alloys. As present, the degree of alloying significantly affected the VBS of Ag_xCu_{100-x} alloys. The DOS near Fermi level, between 1eV and 3eV, is increased with the increasing of Cu content (at.%) in Ag_xCu_{100-x} alloys, which indicates that the position of d-band tend to upshift along with the increasing Cu content.

2.3 The volcano curve for the $Ag_{75}M_{25}$ and Ag_xCu_{100-x} alloys

These d-band centers of VBS allow us to directly correlate the variations in the ORR catalytic activity with the alloying element variations in $Ag_{75}M_{25}$ alloys. **Figure 2c** indicates that the d-band center of $Ag_{75}M_{25}$ versus the specific activity at $0.85V_{RHE}$ exhibit a volcano curve. After alloying with M (Cu, Co and Fe) metallic element, all of the d-band center of $Ag_{75}M_{25}$ alloys are upshifted relative to pure Ag while the ORR activity of Ag catalyst is modified by alloying with M (Cu, Co and Fe) metals. Nevertheless, the relationship of d-band center and ORR activity in $Ag_{75}M_{25}$ alloys is not merely a linear one. Here, the d-band center of $Ag_{75}Cu_{25}$, $Ag_{75}Fe_{25}$ and $Ag_{75}Co_{25}$ is at -5.16 eV, -4.71 eV and -4.45 eV, respectively, whereas their ORR specific activity is 0.23 mA cm^{-2}, 0.177 mA cm^{-2} and 0.112 mA cm^{-2}, respectively, indicating that the ORR activity decreases when the position of the d-band center of $Ag_{75}M_{25}$ becomes extremely close to the Fermi energy, due to that the higher binding energy of OCS (oxygen containing species, such as O_2, OH^-, OOH^-) on Ag surface which blocks the catalytic active site on the surface.[5a, 5b] But for $Ag_{75}In_{25}$ alloy, the downshift of d-band center decreases the binding energy of Ag-OCS which would weaken the ORR activity of Ag.[5a, 5b] This leads to the maximum possible catalytic activity obtained for

the $Ag_{75}Cu_{25}$ alloy, which binds the OCS neither too weakly nor too strongly, indicating a balance between the adsorption energies of reactive intermediates and surface coverage by blocking species. It is interesting to note that, the ORR enhancement of $Ag_{75}M_{25}$ alloys originates from the upshift in d-band center and the upshift amount in d-band center of the most active $Ag_{75}Cu_{25}$ is about 0.12eV relative to pure Ag, but for Pt-M alloys, the ORR enhancement comes from the downshift in the d-band center, for example, the d-band center of the most active Pt-Y,[5a, 14] Pt-Co alloy[15] and Pt-Ni alloy[16] downshifts relative to pure Pt about 0.14eV, 0.20eV and 0.19 eV, respectively, indicating that the tuning of the catalytic enhancement via electronic perturbation in Ag-M alloys is opposite to that of Pt-M alloys.

As shown in **Figure 2d**, the relationship between the specific activity at $0.85V_{RHE}$ and the d-band center positions on Ag_xCu_{100-x} alloys exhibits a volcano shape too, with the maximum catalytic activity obtained for $Ag_{50}Cu_{50}$ (1.57 $mAcm^{-2}$), indicating that ORR activity of Ag_xCu_{100-x} alloys is depends on the alloying degree and the position of d-band states relative to Fermi level. In Cu content range lower than 50 at%, the ORR activity of Ag_xCu_{100-x} alloys increases with the upshifting of d-band center, which enhances the Ag-OCS bond interaction and the ORR activity.[3b] For high Cu content regime (higher than 50%), the ORR activity of Ag_xCu_{100-x} alloys exhibit a significant decrease from 1.57 mA cm^{-2} to 0.55 mA cm^{-2} with increasing Cu content. Further study of XPS surface composition analysis indicates that the content of Cu is 72.11% on the surface of $Ag_{25}Cu_{75}$ alloys and these excess surface Cu atoms get easily oxidized in alkaline solution, which lead to higher dissociation energy for ORR, block the activation site of the Ag atoms, and decrease the ORR activity of Ag_xCu_{100-x} alloys.[3b] The ORR activity of $Ag_{50}Cu_{50}$ is at the top of volcano curve and suggests that this alloy composition has the best balance of the d-band center and surface active site of Ag, which renders it the highest activity for ORR among all compositions.

2.4.The typical microstructure and activity order of the $Ag_{75}M_{25}$ alloys

As measured above, the activity order of these $Ag_{75}M_{25}$ alloys ($Ag_{75}Cu_{25}$> $Ag_{75}Fe_{25}$> $Ag_{75}Co_{25}$) in this work is different with the activity order predicted from the (111) surface ($Ag_{75}Fe_{25}$> $Ag_{75}Co_{25}$> $Ag_{75}Cu_{25}$).[6] To evaluate this argument, we measured the surface characters of these alloys. **Figure 3a** and **Figure S7** present the typical microstructure of these as-prepared catalysts measured by high resolution transmission electron microscope (HRTEM). As an example, the $Ag_{75}Cu_{25}$ particles are ranged from 1 nm to 3.5 nm and present many clearly lattice fringes on the surface. In **Figure 3b**, the inverse FFT of a particle exhibit that the surface of nanoparticles possess several difference lattice plane with d-spacing = 0.238 nm, 0.147 nm and 0.203 nm, which can be indexed to (111), (220) and (200) facets, respectively. As shown in **Figure 3c**, diffraction rings in selected area electron diffraction (SAED) also present the rings from (111), (220) and (200) faces, which is in agreement with the inverse FFT results. These results indicated the $Ag_{75}Cu_{25}$ catalysts have various facets as the active surface. Previous research suggests that the catalytic reaction is not limited to (111) face but occurs also on (200)/(100), (220)/(110) and other faces.[7d, 17] These various active facets in $Ag_{75}Cu_{25}$ alloys may result in a difference activity order with that calculated via DFT on (111) facet.[16] Meanwhile the surface composition and stability of as-prepared Ag-M catalysts were measured by XPS. As present in **Figure 3d** and **3e**, all samples exhibited a clear Ag peak and doping element (M) peaks which can be index to Ag^0 and M^0 metallic state (more details of XPS are shown in supporting information, see **Figure S8**).[18] These results suggest that the Ag-M alloys used in this work have a clean and well alloyed surface.

2.5. The long-term stability of the typical $Ag_{75}M_{25}$ catalysts

Considering the low stability of Ag_9Cu_1/CNT as reported by Yi et al,[8] the long-term stability of $Ag_{75}Cu_{25}$ alloys was measured in this work. The electrochemical durability of the $Ag_{75}Cu_{25}$ catalyst was evaluated by using a line scan voltammetric accelerated stability test (LSV-AST) between 0.6 and 1.0 V (vs RHE) in O_2-saturated 0.1 M KOH at a scan rate of 50

mV s^{-1}. The ORR polarization curves of the $Ag_{75}Cu_{25}$ catalyst after 9000 cycles are shown in **Figure 4a**. (details after each 1000 cycles were showed in supporting information, **Figure S9**). As present, after 9000 cycles, there was a slight decrease in half-wave potential for $Ag_{75}Cu_{25}$ alloy from 0.76 V_{RHE} to 0.75 V_{RHE}. The ORR polarization curve after 9000 cycles present a peak at 0.3V_{RHE}, indicating an obvious difference of the diffusion limiting current. Similar phenomena [6] has been reported in Ag-Co system that the Ag catalyst is sensitive to the electrolyte purity and the long term LSV-AST would influence the limit current of ORR polarization curve. **Figure 4b** and **Table S3** shows the the specific activity and ECSA of the $Ag_{75}Cu_{25}$ catalyst investigated every 1000 cycles by Pb-stripping measurement, the ECSA decrease from 16.49 m^2 g_{total}^{-1} to 14.24 m^2 g_{total}^{-1} after LSV-AST cycles, the specific activity of $Ag_{75}Cu_{25}$ alloy decreases from 0.851 mA cm^{-2} to 0.834 mA cm^{-2} during the LSV-AST cycles, its final specific activity was still as high as 0.834 mA cm^{-2}, which is 2.8-fold higher than the initial value of pure Ag catalyst, suggesting that the $Ag_{75}Cu_{25}$ catalyst has excellent long-term durability.

3. Conclusions

We have demonstrated that the relationships between specific activity and d-band center values in $Ag_{75}M_{25}$ and Ag_xCu_{100-x} alloys exhibit a volcano shape. From the volcano curve of $Ag_{75}M_{25}$ alloys, we have established a new activity order for these alloys as $Ag_{75}Cu_{25}$ > $Ag_{75}Fe_{25}$ > $Ag_{75}Co_{25}$> Ag> $Ag_{75}In_{25}$. The activity study shows that the slight upshift in d-band center, approximately 0.12 eV, is beneficial for ORR activity in $Ag_{75}M_{25}$ system. This result is in contrast to Pt-based alloys where the slight downshift (approximately 0.14 eV for Pt-Y) of d-band center improves ORR activity. For $Ag_{75}M_{25}$ alloys, the $Ag_{75}Cu_{25}$ exhibits the most activity with the best balance of the binding energy of oxygen and anions. We also studied the effect of copper content in the Ag_xCu_{100-x} alloys and found a volcano curve for activity plot relative to Cu content. These results indicate that activity enhancement of Ag_xCu_{100-x} alloys depend on the degree of alloying. Though Cu is suitable for modifying the

d-band center of Ag, excessive Cu on surface will block the active sites on Ag_xCu_{100-x} surface and deteriorate the catalytic activity. Our results indicate that the $Ag_{50}Cu_{50}$ alloy is most active among Ag_xCu_{100-x} alloys due to best balance between d-band position and the surface Cu content. Moreover, the LSV-AST results confirm that the $Ag_{75}Cu_{25}$ catalyst is stable in alkaline solution even after 9000 cycles, indicating its excellent ORR stability. This work suggests that it is feasible to increase the catalytic activity and stability of the Ag-based nanoparticles by tuning the electronic properties, resulting in a new generation of Ag-Cu systems with engineered alloying.

4. Materials and methods

4.1. Catalyst preparation.

We prepared polycrystalline nanoalloy catalysts of the type $Ag_{75}M_{25}$ (M=Cu, Co, Fe and In) and Ag_xCu_{100-x} (x=0, 25, 45, 50, 55, 75, 90 and 100) via the pulse laser deposition (PLD, **Figure S1**) technology. This non-equilibrium vapor deposition technique ensures the consistency of these alloys by exactly controlling target composition, evaporating temperature and deposition time (details of this experiment have been shown in supporting information).[19]

The Ag-M alloys were in-situ deposited on glassy carbon electrode (GC, 0.196cm^{-2}) via PLD at 1.0×10^{-5} Pa atmospheric pressure. No binding materials (such as PTFE) and substrates (such as carbon) were used between GC and Ag-M alloys. The GC was first cleaned in dilute sulphuric acid for 5 mins, followed by washing in deionized water for 30 mins and drying in vacuum oven (1 hours). The GC was then directly set on the side of adjustable rotation rate sample platform (ARRSP) of the PLD. The $Ag_{75}M_{25}$ (M=Fe, Co, Cu and In) and Ag_xCu_{100-x}(x=0, 25, 45, 50, 55, 75, 90, 100) sputtering targets were mounted on the side of adjustable rotation rate target platform (ARRTP). Both the ARRSP and ARRTP rotated at the speed of 5 rpm and cooled by flowing Ar during the deposition process. The distance of the ARRSP - to - ARRTP was 6 cm. To clean the surface of the targets, a nanosecond Q-switched Nd laser

irradiation (YAG laser beam with a wavelength of 266 nm and a pulse duration of 3-6 ns, beam diameter 1 mm with an energy density 200 mJ/pulse, EKSPLA, Lithuania) was performed on the targets for 5 minutes at 2Hz. After this steo, the Ag-M targets were allowed to deposit onto the GC at 9 Hz. All of the catalyst samples were deposited with 4400 laser pulses and the thickness and loading of Ag-M alloys on GC is 12μg cm^{-2} as monitored by the quartz crystal oscillation.

4.2. Catalyst characterisation.

X-ray photoelectron spectroscopy (XPS) were measured on an ULTRA (ESCALAB 250, Al Kα,ultrahigh vacuum is 10^{-9}， hν = 1486.6 eV). High-resolution O1s, Cu2p and Ag3d spectra were acquired. No charge compensation was necessary. The origin of the binding energy E_b was set to the Fermi energy E_f of the Au plate. The Shirley background is subtracted from the measured spectra. The d-band center of the valence band (VBS) is given by $\int R(\varepsilon)\varepsilon d\varepsilon / \int R(\varepsilon) d\varepsilon$, where the R(ε) is the XPS-intensity after background subtraction.[14] The structural of the synthesized catalysts were determined using an FEI Tecnai F30 transmission electron microscope (300 kV), a JEOL JSM-6700F field-emission scanning electron microscope.

All electrochemical measurements were carried out by a classic three electrode set-up. The Hg/HgO (0.1M) electrode was used as a reference electrode, a Pt wire electrode was employed as a counter electrode. The working electrodes were fabricated by directly depositing Ag-M alloys on GC. The catalyst loading was 12 μg cm^{-2}. Electrolyte solutions of 0.1 M KOH were prepared from ultrapure water (18.1MΩ cm^{-1}) and 99.999% potassium hydroxide. All solutions were freshly prepared before use and stored in a glove box to avoid the contamination from the air (such as CO_2). We considered IR-dropping in all of the tests. All potentials are reported relative to the Reversible Hydrogen Electrode ($V_{RHE} = V_{NHE} + 0.0591pH$).[6] The rotating disk electrode (RDE) and CHI660C electrochemical workstation were performed to measure the electrocatalytic activity of the catalysts. The linear

voltammetry scanning (LSV) and rotating disk electrode (RDE) polarization curves were studied at room temperature in 0.1 M KOH(O_2 saturated). The scanning rate of these experiments were set as 10 mV s^{-1} and the rotation rates were controlled at 400, 900, 1600 and 2500 rpm.

Pb-stripping voltammetry was performed immediately after ORR measurements in 0.1M KOH+125μM $Pb(NO_3)_2$ solution. Before Pb-stripping voltammetry test, the solution was purged with Ar for 30 minutes. The initial potential were set at 0.2V_{RHE} and the final potential is 0.6 V_{RHE}. The stable voltammograms were integrated assuming 280uC/cm^2, which was established based on Ag faces.[20]

Supporting Information

Supporting Information is available from the Wiley Online Library or from the author.

Acknowledgments

This study was supported by the National Natural Science Foundation of China (grant nos. 51271148 and 50971100), the Research Fund of State Key Laboratory of Solidification Processing in China (grant no. 150-ZH-2016), the Aeronautic Science Foundation Program of China (grant no. 2012ZF53073), the Science and Technology Innovation Fund of Western Metal Materials (grant no. XBCL-2-11) and the Doctoral Fund of Ministry of Education of China (grant no. 20136102110013).

References

1. a) L.Q. Mao; D. Zhang; T. Sotomura; K. Nakatsu; N. Koshiba; T. Ohsaka, *Electrochim. Acta* **2003,** *48*, 1015-1021; b) D.L. Wang; H.L. Xin; Y.C. Yu; H.S. Wang; E. Rus; D.A. Muller; H.D. Abruna, *J. Am. Chem. Soc.* **2010,** *132*, 17664-17666.
2. a) M. Chatenet; L. Genies-Bultel; M. Aurousseau; R. Durand; F. Andolfatto, *Appl. Electrochem.* **2002,** *32*, 1131-1140; b) Y. Li; H. Dai, *Chem. Soc. Rev.* **2014,** *43*, 5257-75; c) A. Qaseem; F. Chen; X. Wu; R.L. Johnston, *Catal. Sci. Technol.* **2016**.
3. a) T. Hofmann; T.H. Yu; M. Folse; L. Weinhardt; M. Bär; Y. Zhang; B.V. Merinov; D.J. Myers; W.A. Goddard; C. Heske, *J. Phys. Chem. C* **2012,** *116*, 24016-24026; b) K. Shin; D.H. Kim; S.C. Yeo; H.M. Lee, *Catal. Today* **2012,** *185*, 94-98; c) N. Wagner; M. Schulze; E. Gülzow, *J. Power Sources* **2004,** *127*, 264-272; d) J.L. Fernandez; D.A. Walsh; A.J. Bard, *J. Am. Chem. Soc.* **2005,** *127*, 357-365; e) F.H.B. Lima; J.F.R. de Castro; E.A. Ticianelli, *J. Power Sources* **2006,** *161*, 806-812.
4. a) X.Q. Wu; F.Y. Chen; N. Zhang; A. Qaseem; R.L. Johnston, *J. Mater. Chem. A* **2016,** *4*, 3527-3537; b) X.Q. Wu; F.Y. Chen; Y.C. Jin; N. Zhang; R.L. Johnston, *ACS Appl. Mater. Interfaces* **2015,** *7*, 17782-17791.
5. a) S. Jong Yoo; S.K. Kim; T.Y. Jeon; S. Jun Hwang; J.G. Lee; S.C. Lee; K.S. Lee; Y.H. Cho; Y.E. Sung; T.H. Lim, *Chem. Commun.* **2011,** *47*, 11414-6; b) Y.T. Liang; S.P. Lin; C.W. Liu; S.R. Chung; T.Y. Chen; J.H. Wang; K.W. Wang, *Chem. Commun.* **2015,** *51*, 6605-6608; c) V. Stamenkovic; B.S. Mun; K.J.J. Mayrhofer; P.N. Ross; N.M. Markovic; J. Rossmeisl; J. Greeley; J.K. Nørskov, *Angew. Chem.* **2006,** *118*, 2963-2967.
6. A. Holewinski; J.C. Idrobo; S. Linic, *Nat. Chem.* **2014,** *6*, 828-34.
7. a) B. Lim; M.J. Jiang; P.H.C. Camargo; E.C. Cho; J. Tao; X.M. Lu; Y.M. Zhu; Y.N. Xia, *Science* **2009,** *324*, 1302-1305; b) D.Y. Wang; H.L. Chou; C.C. Cheng; Y.H. Wu; C.M. Tsai; H.Y. Lin; Y.L. Wang; B.J. Hwang; C.C. Chen, *Nano Energy* **2015,** *11*, 631-639; c) Q.Y. Wang; X.Q. Cui; W.M. Guan; L. Zhang; X.F. Fan; Z. Shi; W.T. Zheng, *J. Power Sources* **2014,** *269*, 152-157; d) L. Bu; J. Ding; S. Guo; X. Zhang; D. Su; X. Zhu; J. Yao; J. Guo; G. Lu; X. Huang, *Adv. Mater.* **2015,** *27*, 7204-12.
8. Q.F. Yi; H. Chu; M.X. Tang; Z. Yang; Q.H. Chen; X.P. Liu, *J. Electroanal. Chem.* **2015,** *739*, 178-186.
9. K. Shin; H. Kim da; H.M. Lee, *ChemSusChem* **2013,** *6*, 1044-9.
10. N. Zhang; F.Y. Chen; X.Q. Wu, *Sci. Rep.* **2015,** *5*.
11. a) Y.C. Jin; F.Y. Chen; Y.M. Lei; X.Q. Wu, *Chemcatchem* **2015,** *7*, 2377-2383; b) Y.C. Jin; F.Y. Chen, *Electrochim. Acta* **2015,** *158*, 437-445.
12. X.Z. Li; Y.Y. Fang; X.Q. Lin; M. Tian; X.C. An; Y. Fu; R. Li; J. Jin; J.T. Ma, *J. Mater. Chem. A* **2015,** *3*, 17392-17402.
13. a) J. Masa; C. Batchelor-McAuley; W. Schuhmann; R.G. Compton, *Nano Res.* **2014,** *7*, 71-78; b) Y. Lu; Y. Wang; W. Chen, *J. Power Sources* **2011,** *196*, 3033-3038; c) R.R. Chen; H.X. Li; D. Chu; G.F. Wang, *J. Phys. Chem. C* **2009,** *113*, 20689-20697.
14. S.J. Hwang; S.K. Kim; J.G. Lee; S.C. Lee; J.H. Jang; P. Kim; T.H. Lim; Y.E. Sung; S.J. Yoo, *J. Am. Chem. Soc* **2012,** *134*, 19508-11.
15. V.R. Stamenkovic; B.S. Mun; M. Arenz; K.J. Mayrhofer; C.A. Lucas; G. Wang; P.N. Ross; N.M. Markovic, *Nat. Mater.* **2007,** *6*, 241-7.
16. V. Stamenkovic; B.S. Mun; K.J.J. Mayrhofer; P.N. Ross; N.M. Markovic; J. Rossmeisl; J. Greeley; J.K. Norskov, *Angew Chem. Int. Ed.* **2006,** *45*, 2897-2901.
17. a) Y. Zhou; Q. Lu; Z.B. Zhuang; G.S. Hutchings; S. Kattel; Y.S. Yan; J.G.G. Chen; J.Q. Xiao; F. Jiao, *Adv. Energy Mater.* **2015,** *5*; b) V.R. Stamenkovic; B. Fowler; B.S. Mun; G. Wang; P.N. Ross; C.A. Lucas; N.M. Markovic, *Science* **2007,** *315*, 493-7.
18. F.M. John; F.S. William; E.S. Peter; D.B. Kenneth, *Handbook of X-ray Photoelectron Spectroscopy*. Perkin-Elmer Corporation Physical Electronics Division: Eden Prairie: Unite states of America, 1992; p 261.
19. S.J. Chung; A. Roy; D.H. Hong; J.P. Leonard; P.N. Kumta, *Mater. Sci. Eng. B* **2011,** *176*, 1690-1694.
20. E. Kirowa-Eisner; D. Tzur; E. Gileadi, *J. Electroanalyt. Chem.* **2008,** *621*, 146-158.

Table 1. The ORR activity parameters: half-wave potential(E_{half}), kinetic currents(j_{kc}), mass-corrected kinetic current(j_{mass}), electrochemical surface areas (ECSA, $m^2 g_{total}^{-1}$) and Tafel slopes (mV dec^{-1})of the $Ag_{75}M_{25}$ and Ag_xCu_{100-x} catalysts in O_2-saturated 0.1 M KOH in positive direction at scan rate of 10 mVs^{-1} and with electrode rotation frequency of 1600 rpm.

Catalyst		Half-wave potential (V_{RHE})	Current density (mA cm^{-2})			Mass-corrected kinetic current at 0.85V_{RHE} (A g_{total}^{-1})	ECSA (m^2 g_{total}^{-1})	Tafel plots (mV dec^{-1})	
		E_{half}	j	j_d	j_{kc}	j_{mass}	A	Low overpotentials	High overpotentials
$Ag_{75}M_{25}$	Ag	0.66	0.3	4.12	0.32	26.7	14.05	79	138
	$Ag_{75}In_{25}$	0.56	0.01	4.20	0.01	0.8	15.22	81	147
	$Ag_{75}Co_{25}$	0.70	0.64	4.14	0.76	63.3	15.79	78	131
	$Ag_{75}Fe_{25}$	0.73	0.75	4.15	0.92	76.7	15.65	76	129
	$Ag_{75}Cu_{25}$	0.76	0.85	4.19	1.07	89.5	16.49	72	108
Ag_xCu_{100-x}	$Ag_{90}Cu_{10}$	0.69	0.47	4.16	0.53	44.2	15.56	78	110
	$Ag_{55}Cu_{45}$	0.81	1.28	4.21	1.85	154.2	15.93	69	106
	$Ag_{50}Cu_{50}$	0.82	1.57	4.21	2.49	207.5	16.90	64	104
	$Ag_{45}Cu_{55}$	0.81	1.49	4.15	2.33	194.2	16.43	59	106
	$Ag_{25}Cu_{75}$	0.71	0.55	4.13	0.63	52.5	15.93	75	112
	Pt/C-20%	0.88	1.72	4.23	2.90	241.6	--	58	64

j of $Ag_{75}M_{25}$ and Ag_xCu_{100-x} catalysts is the total current density at 0.85 V_{RHE}, j of Pt/C-20% is the total current density at 0.90 V_{RHE}.
j_d is the diffusion limited current density
j_{kc} is the kinetic current at 0.85V_{RHE}.
j_{mass} is the mass-corrected kinetic current at 0.85V_{RHE}.

Table 2. The position of d-band centre and specific activity (SA) of the $Ag_{75}M_{25}$ and Ag_xCu_{100-x} catalysts

Catalyst		Position of d-band center, E_d (eV)	Up-shift d-band Center, ΔE_d (eV)	SA at 0.85V_{RHE} J_s (mA cm^{-2})	Improvement of SA ΔJ_s (mA cm^{-2})
$Ag_{75}M_{25}$	Ag	-5.28	0	0.3	0
	$Ag_{75}In_{25}$	-5.51	-0.23	0.01	-0.29
	$Ag_{75}Co_{25}$	-4.45	0.83	0.64	0.34
	$Ag_{75}Fe_{25}$	-4.71	0.57	0.75	0.45
	$Ag_{75}Cu_{25}$	-5.16	0.12	0.95	0.65
Ag_xCu_{100-x}	$Ag_{90}Cu_{10}$	-5.21	0.07	0.47	0.17
	$Ag_{55}Cu_{45}$	-4.98	0.30	1.28	0.98
	$Ag_{50}Cu_{50}$	-4.92	0.36	1.57	1.27
	$Ag_{45}Cu_{55}$	-4.8	0.48	1.49	1.19
	$Ag_{25}Cu_{75}$	-4.7	0.58	0.55	0.25

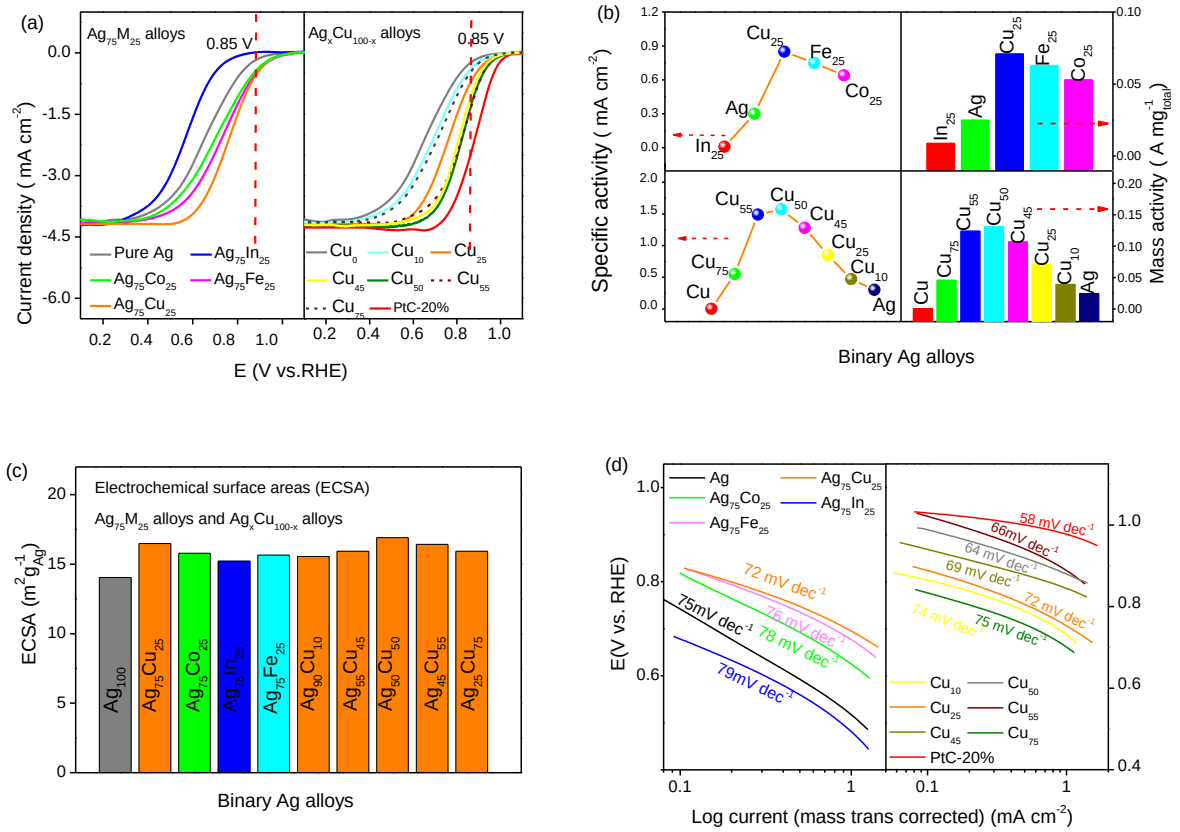

Figure 1. (a) The ORR polarization curves of $Ag_{75}M_{25}$ (M: Cu, Co, Fe and In) alloys, Ag_xCu_{100-x} (x= 0, 25, 45, 50, 55, 75, 90 and 100) alloys ; Electrolyte: O_2 saturated 0.1M KOH solution, room temperature; sweep rate, 10 mV s^{-1}; rotation rate, 1600 rpm; loading of $Ag_{75}M_{25}$ and Ag_xCu_{100-x} : 12 μg cm^{-2}. (b) Relationships between experimentally measured specific activity (SA) and mass activity (MA) of $Ag_{75}M_{25}$, and Ag_xCu_{100-x} alloys at $0.85V_{RHE}$ versus the compositions of M. (c) The corresponding electrochemical surface areas (ECSA) of $Ag_{75}M_{25}$ and Ag_xCu_{100-x} alloys. (d) The mass-transport corrected kinetic current Tafel plots for the $Ag_{75}M_{25}$ and Ag_xCu_{100-x} alloys.

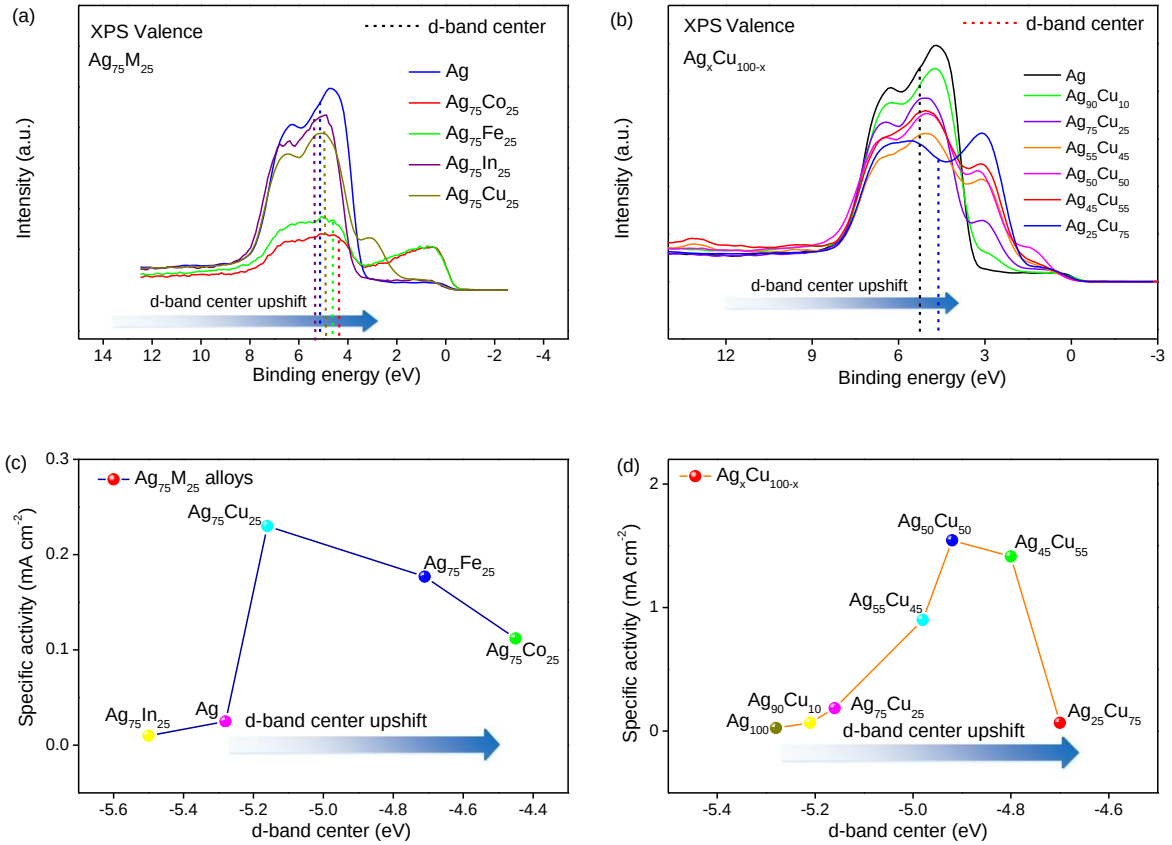

Figure 2. Valence band spectra (VBS) of (a) the $Ag_{75}M_{25}$ and (b) Ag_xCu_{100-x} alloys as measured by high-resolution X-ray photoelectron spectroscopy. (c) Relationships between experimentally measured specific activity (SA) at $0.85V_{RHE}$ versus the d-band center position for $Ag_{75}M_{25}$ alloys with various kinds of alloy composition. (d) Relationships between specific activity (SA) at $0.85V_{RHE}$ versus the d-band center position for Ag_xCu_{100-x} alloys with various content of Cu.

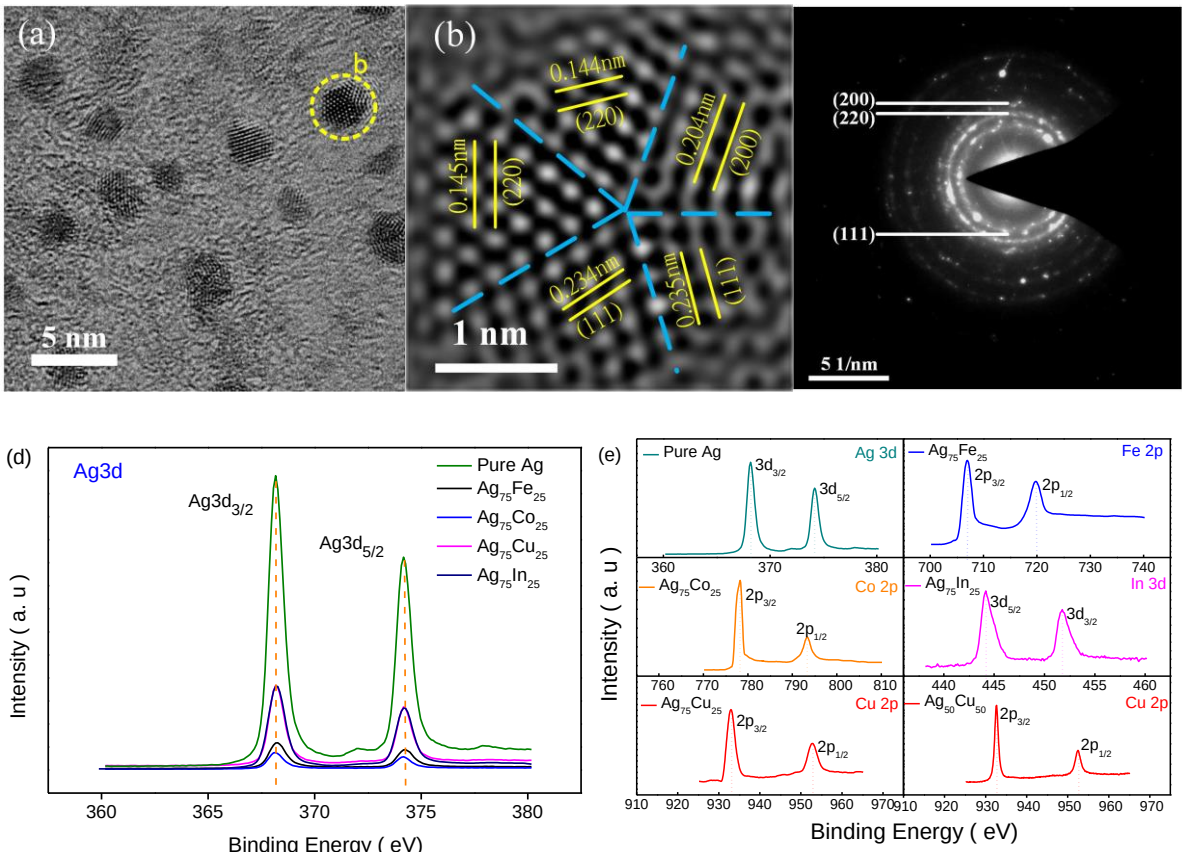

Figure 3. (a) Typical HRTEM images of the Ag-M ($Ag_{75}Cu_{25}$) alloy, (b) the inverse FFT for the particle b, (c) typical selected area electron diffraction (SAED) of the Ag-M alloy ($Ag_{75}Cu_{25}$) alloy, (d) XPS of Ag3d regions for pure Ag, $Ag_{75}Fe_{25}$, $Ag_{75}In_{25}$, $Ag_{75}Co_{25}$ and $Ag_{75}Cu_{25}$ alloys, (e) XPS of Ag 3d, Fe 2p, Co 2p, Cu 2p and In 3d regions for Pure Ag, $Ag_{75}Fe_{25}$, $Ag_{75}Co_{25}$, $Ag_{75}In_{25}$, $Ag_{75}Cu_{25}$ and $Ag_{50}Cu_{50}$ alloys.

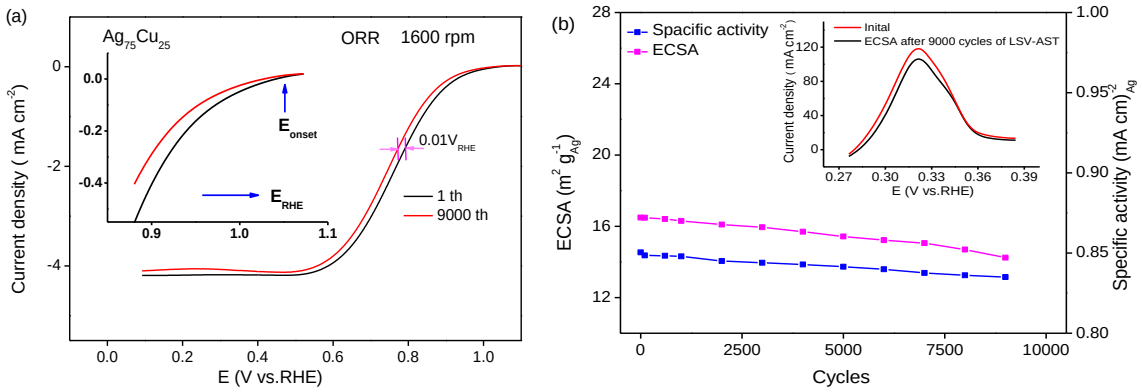

Figure 4. (a) A comparison of ORR polarization curves before and after 9000 cycles of line scan voltammetric accelerated stability tests (LSV-AST) for the $Ag_{75}Cu_{25}$ catalysts in O_2-saturated 0.1 M KOH; sweep rate was 10 mVs^{-1} and rotating rate was 1600 rpm. (b) The corresponding electrochemical surface areas (ECSA) and specific activity (SA) of $Ag_{75}Cu_{25}$ catalysts on each stage of LSV-AST.

The ORR activity trends of binary silver alloy nanocatalysts were discussed, which is highly dependence on the d-band center of valence band spectrum. The results present that the up shift d-band center is benefit for ORR and the optimal $Ag_{50}Cu_{50}$ catalyst (0.1eV) shows highly activity and durability for ORR in alkaline media, which is comparable to the commercial Pt/C-20% catalyst.

Keyword: binary silver alloy, activity trends, d-band center, valence band spectrum

Xiaoqiang Wu,[a] Fuyi Chen,[a] Nan Zhang,[a] Yimin Lei,[a] Yachao Jin,[a] Adnan Qaseem,[a] and Roy L. Johnston[b]*

Activity Trends of Binary Silver Alloy Nanocatalysts for Oxygen Reduction Reaction in Alkaline Media

TOC:

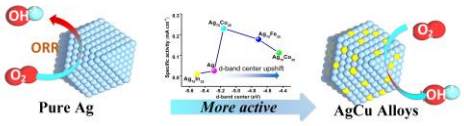

Supporting Information

Activity Trends of Binary Silver Alloy Nanocatalysts for Oxygen Reduction Reaction in Alkaline Media

Xiaoqiang Wu,[a] Fuyi Chen,[a] Nan Zhang,[a] Yimin Lei,[a] Yachao Jin,[a] Adnan Qaseem,[a] and Roy L. Johnston[b]*

Part 1. Preparation of the Ag-M alloys.

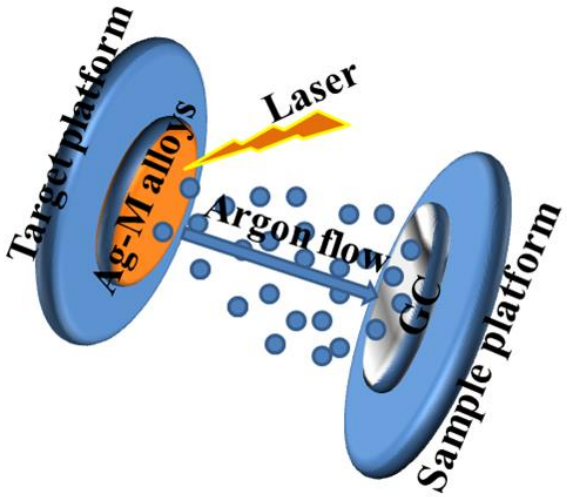

Figure S1. Preparation of Ag-M electrodes.

To ensure the accuracy of the experimental results, the Ag-M alloys were in-situ deposited on glassy carbon electrode (GC, 0.196cm^{-2}) via pulse laser deposition (PLD) at 1.0×10^{-5} Pa atmospheric pressure. No binding materials (such as PTFE) and substrates (such as carbon) were used between GC and Ag-M alloys. The GC was first cleaned in dilute sulphuric acid for 5 mins, followed by washing in deionized water for 30 mins and drying in vacuum oven (1 hours). The GC was then directly set on the side of adjustable rotation rate sample platform (ARRSP) of the PLD. The $Ag_{75}M_{25}$ (M=Fe, Co, Cu and In) and Ag_xCu_{100-x}(x=0, 25, 45, 50, 55, 75, 90, 100) sputtering targets were fixed on the side of adjustable rotation rate target platform (ARRTP). Both the ARRSP and ARRTP rotated at the speed of 5 rpm and cooled by flowing Ar during the deposition process. The distance of the ARRSP - to - ARRTP was 6cm. To clean the surface of the targets, nanosecond Q-switched Nd laser irradiation (YAG laser beam with a wavelength of 266 nm and a pulse duration of 3-6 ns, beam diameter 1 mm with an energy density 200 mJ/pulse, EKSPLA, Lithuania) was performed on the targets for 5 minutes at 2Hz. After this process, the Ag-M targets were allowed to deposit onto the GC at 9 Hz. All of the catalyst samples were deposited with 4400 laser pulses(The loading of Ag-M alloys on GC is 12μg cm^{-2}).

Part 2. Electrochemical measurements

Oxygen reduction reaction tests (ORR)

All electrochemical measurements were carried out by a classic three electrode set-up. The Hg/HgO (0.1M) electrode was used as a reference electrode, a Pt wire electrode was employed as a counter electrode. The working electrodes were fabricated by directly depositing Ag-M alloys on GC. The catalyst loading was 12 μg cm^{-2}. Electrolyte solutions of 0.1 M KOH were prepared from ultrapure water (18.1MΩ cm^{-1}) and 99.999% potassium hydroxide. All solutions were freshly prepared before use and stored in a glove box to avoid the contamination from the air (such as CO_2). We considered IR-dropping in all of the tests. All potentials are reported relative to the Reversible Hydrogen Electrode($V_{RHE}=V_{NHE}+0.0591pH$).[1] The rotating disk electrode (RDE) and CHI660C electrochemical workstation were performed to measure the electrocatalytic activity of the catalysts. The linear voltammetry scanning (LSV) and rotating disk electrode (RDE) polarization curves were studied at room temperature in 0.1 M KOH(O_2 saturated). The scanning rate of these experiments were set as 10 mV s^{-1} and the rotation rates were controlled at 400, 900, 1600 and 2500 rpm.

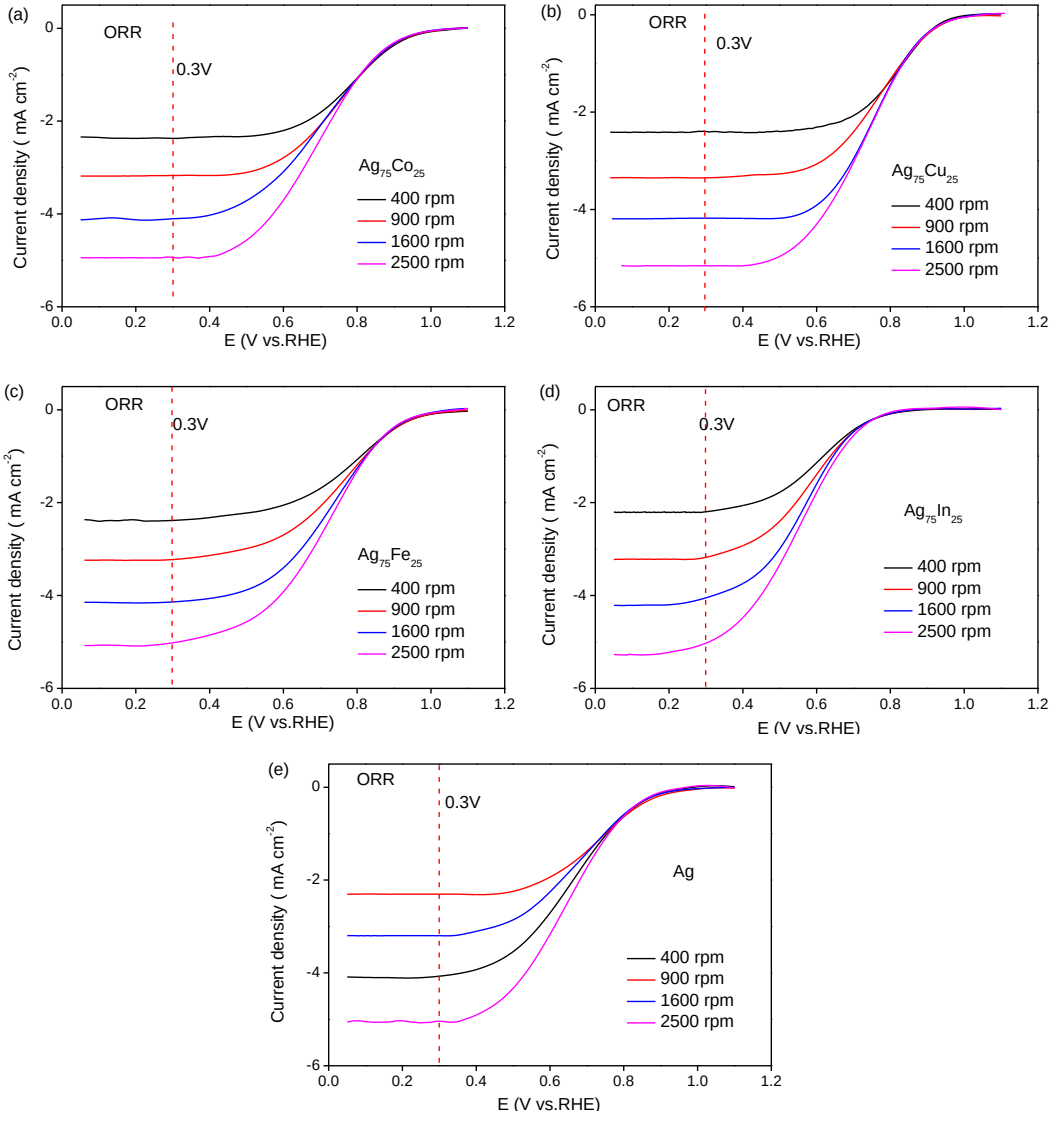

Figure S2. The ORR polarization curves of $Ag_{75}M_{25}$ alloys.

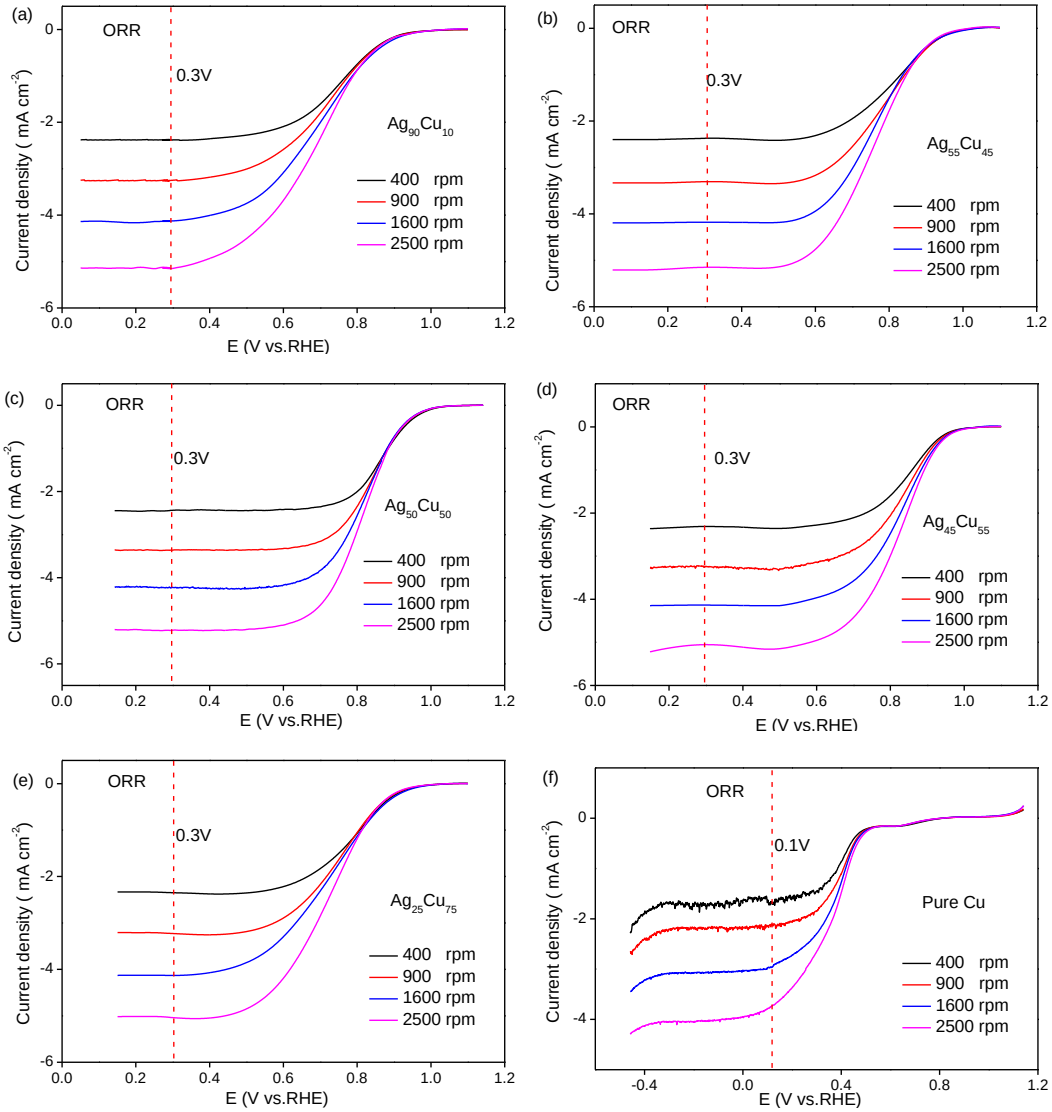

Figure S3. The ORR polarization curves of Ag_xCu_{100-x} alloys.

Koutecky-Levich (KL) analysis and Tafel plots

The Koutecky-Levich equation was applied to calculate kinetic current density based on ORR polarization curve. The number (n) of electrons transferred in the ORR process can be obtained from the slope of the Koutecky-Levich plot.[2]

$$j^{-1}=j_k^{-1}+ (0.62nFCD^{2/3}v^{-1/6}\omega^{1/2})^{-1} \quad (1)$$

Where j is the measured electrode current density, j_k is the kinetic current density, and ω is the electrode rotation rate. The value of D is 1.9×10^{-5} cm^2/s, C_0 is 1.2×10^{-6} mol/cm^3, ν is 1.1×10^{-2} cm^2/s, and F is 96485 C/mol.

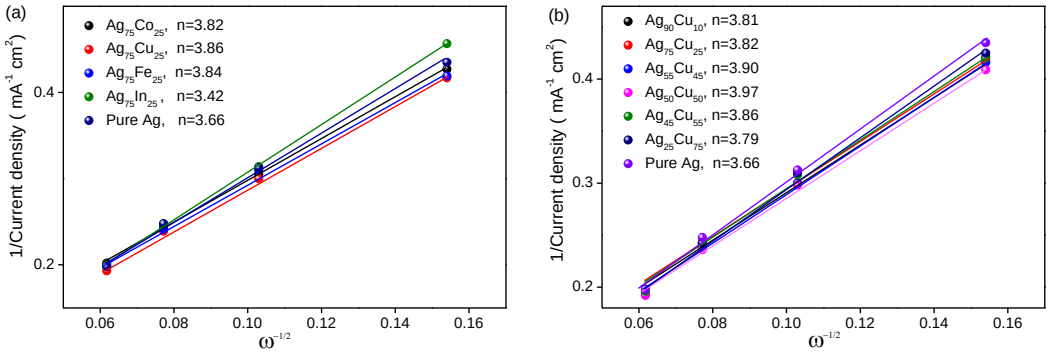

Figure S4. Koutecky-Levich plots collected from corresponding RDE polarization curves of Ag-M alloys at $0.3V_{RHE}$.

Tafel plots analysis

The catalyst film on GC was made thin and smooth via PLD, so that its effect on the kinetic parameters was negligible. Tafel plots were constructed from the corresponding polarization curves, in which the kinetic current densities were calculated by mass-transport correction as follows:[3]

$$J_{kc}=(J_i \times J)\times(J_i - J)^{-1} \qquad (2)$$

where J_i is the diffusion limited current density and J is the real current density as measured in ORR polarization curves.

Electrochemically active surface area (ECSA) analysis

Pb-stripping voltammetry was performed immediately after ORR measurements in 0.1M KOH+125μM $Pb(NO_3)_2$ solution. Before Pb-stripping voltammetry test, the solution was purged with Ar for 30 minutes. The initial potential were set at $0.2V_{RHE}$ and the final potential is 0.6 V_{RHE}. The stable voltammograms were integrated assuming 280μC/cm^2, which was established based on Ag faces.[4] The ECSA were calculated by equation as follow:

$$ECSA=Q_h/280 \quad (3)$$

Where the Q_h is surface charge that can be calculated from the area under the CV by equation as follow:

$$Q_h=\int j(E)\,dE\times(V\times m)^{-1} \quad (3)$$

Where the j(E) is the real current density as shown in Figure S5, V is the scan rate. In this work, the scan rate is 10mV/s.

Table S1. Comparisons of Pb-stripping area, surface charge and ECSA of $Ag_{75}M_{25}$ and Ag_xCu_{100-x} catalysts.

Catalyst		Area of Pb-stripping (A)	Surface charge (Q_h)	ECSA	Change of ECSA relative to pure Ag *ΔECSA*
		$\int j(E)dE$	$\times10^6$ uC	m^2/g_{Ag}	m^2/g_{Ag}
	Ag	472.1	39.33	14.05	0
$Ag_{75}M_{25}$	$Ag_{75}In_{25}$	511.4	42.62	15.22	1.17
	$Ag_{75}Co_{25}$	530.5	44.21	15.79	1.74
	$Ag_{75}Fe_{25}$	525.9	43.83	15.65	1.60
	$Ag_{75}Cu_{25}$	554.0	46.16	16.49	2.44
Ag_xCu_{100-x}	$Ag_{90}Cu_{10}$	521.3	43.45	15.56	1.51
	$Ag_{55}Cu_{45}$	535.4	44.61	15.93	1.88
	$Ag_{50}Cu_{50}$	568.4	47.33	16.90	2.85
	$Ag_{45}Cu_{55}$	552.2	46.02	16.43	2.38
	$Ag_{25}Cu_{75}$	535.4	44.61	15.93	1.88

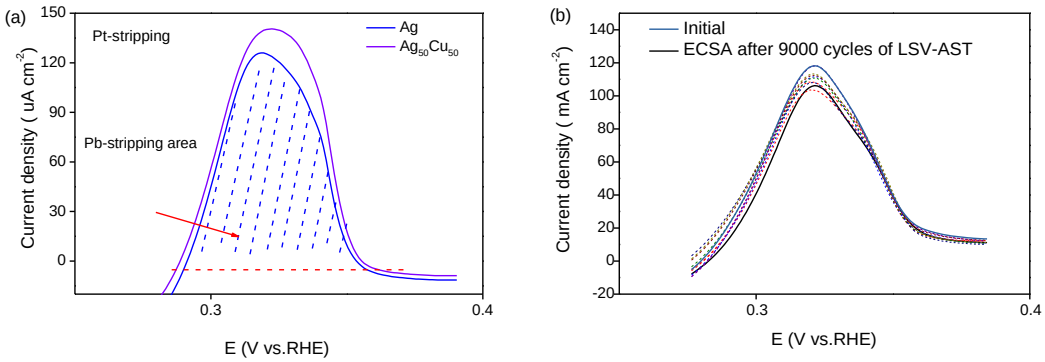

Figure S5. (a) the corresponding electrochemical surface areas (ECSA) of Ag-M alloys. (b) the corresponding ECSA of $Ag_{75}Cu_{25}$ alloy after 100, 600, 1000, 2000, 3000, 4000, 5000, 6000, 7000, 8000 and 9000 cycles accelerated stability test.

Part 3. The model and calculation methods.

The DFT calculations are carried out by using the Dmol3 package. The exchange-correlation potential is treated with the GGA-PBE functional. The orbital cutoff range was set to 5.0 Å and the Fermi smearing was set to 1.0×10^{-5} Ha. The DFT semi-core pseudo potential was used to treat the core electrons of heavy Ag and Cu atoms. The convergence tolerances of energies, forces and displacements were 1.0×10^{5} Ha, 0.002 Ha/Å and 0.005 Å, respectively. We used a periodic slab to model the clean and Cu-decorated Ag(111) surfaces, which were repeated in a (2 × 2) surface unit cell while having four atomic layers and a vacuum gap of 14 Å in the z-direction.

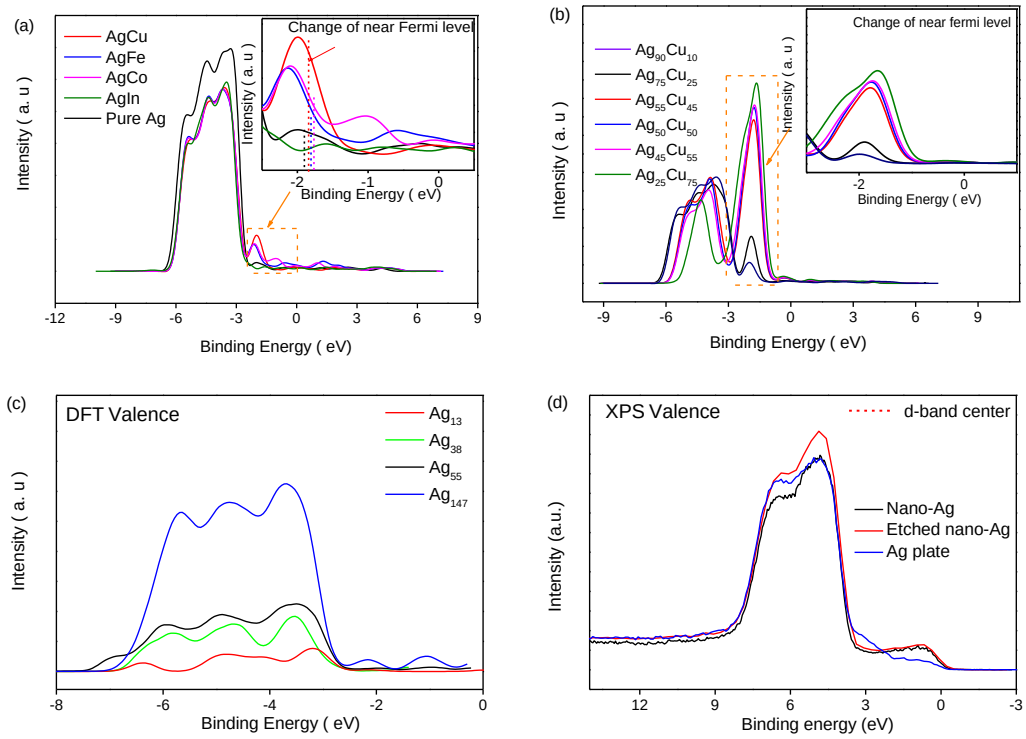

Figur S6. (a) Valence band spectra (VBS) of (a) $Ag_{75}M_{25}$ alloys calculate by density function theory(DTF). (b) Valence band spectra (VBS) of (a) Ag_xCu_{100-x} alloys calculate by density function theory(DTF). (c) VBS of Ag_{13},Ag_38,Ag_{55} and Ag_{147} measured by DFT.(d) The VBS of nano-Ag, etched nano-Ag and Ag plate measured by XPS.

Table S2. **Comparison of the position of d-band centre and change of DOS(near fermi level)**

Catalyst	Position of d-band center E_d (eV)	Up-shift d-band center ΔE_d (eV)	Intensity of DOS (between 0eV to -3eV) $\int R(\varepsilon)d\varepsilon$	Change of DOS (between 0eV to -3eV) $\Delta\int R(\varepsilon)d\varepsilon$	Position of DOS Centre (between 0eV to -3eV) E(eV)
Ag	-4.61	0	3.83	0	-2.47
$Ag_{75}In_{25}$	-4.65	0.04	2.94	-0.89	-2.50
$Ag_{75}Co_{25}$	-4.35	0.26	10.46	6.63	-1.84
$Ag_{75}Fe_{25}$	-4.42	0.19	8.46	4.63	-1.90
$Ag_{75}Cu_{25}$	-4.49	0.12	10.12	6.29	-1.90

*ε is the binding energy; $R(\varepsilon)$ is the intensity of DOS.

Part 4. TEM results of Ag catalyst

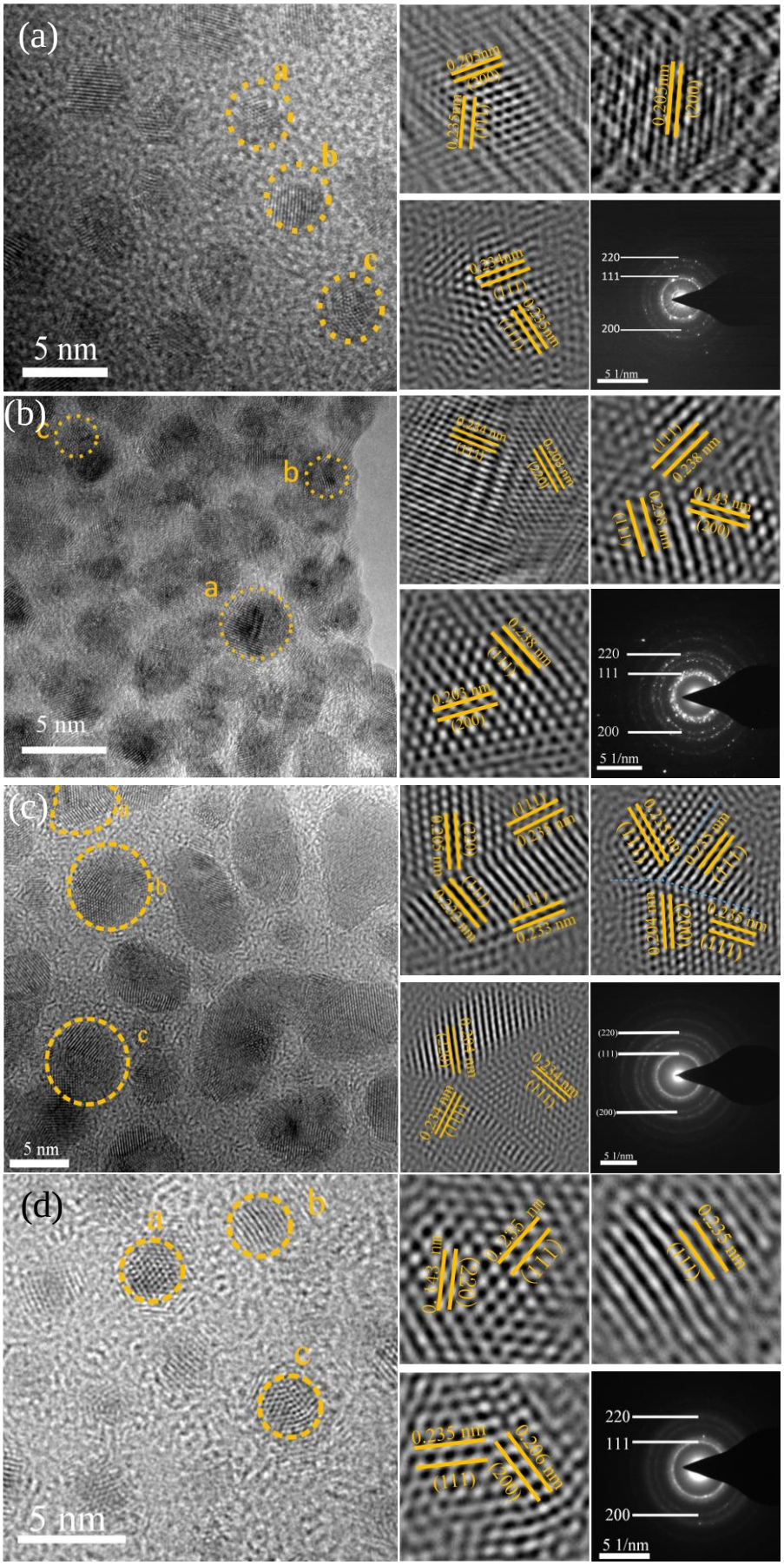

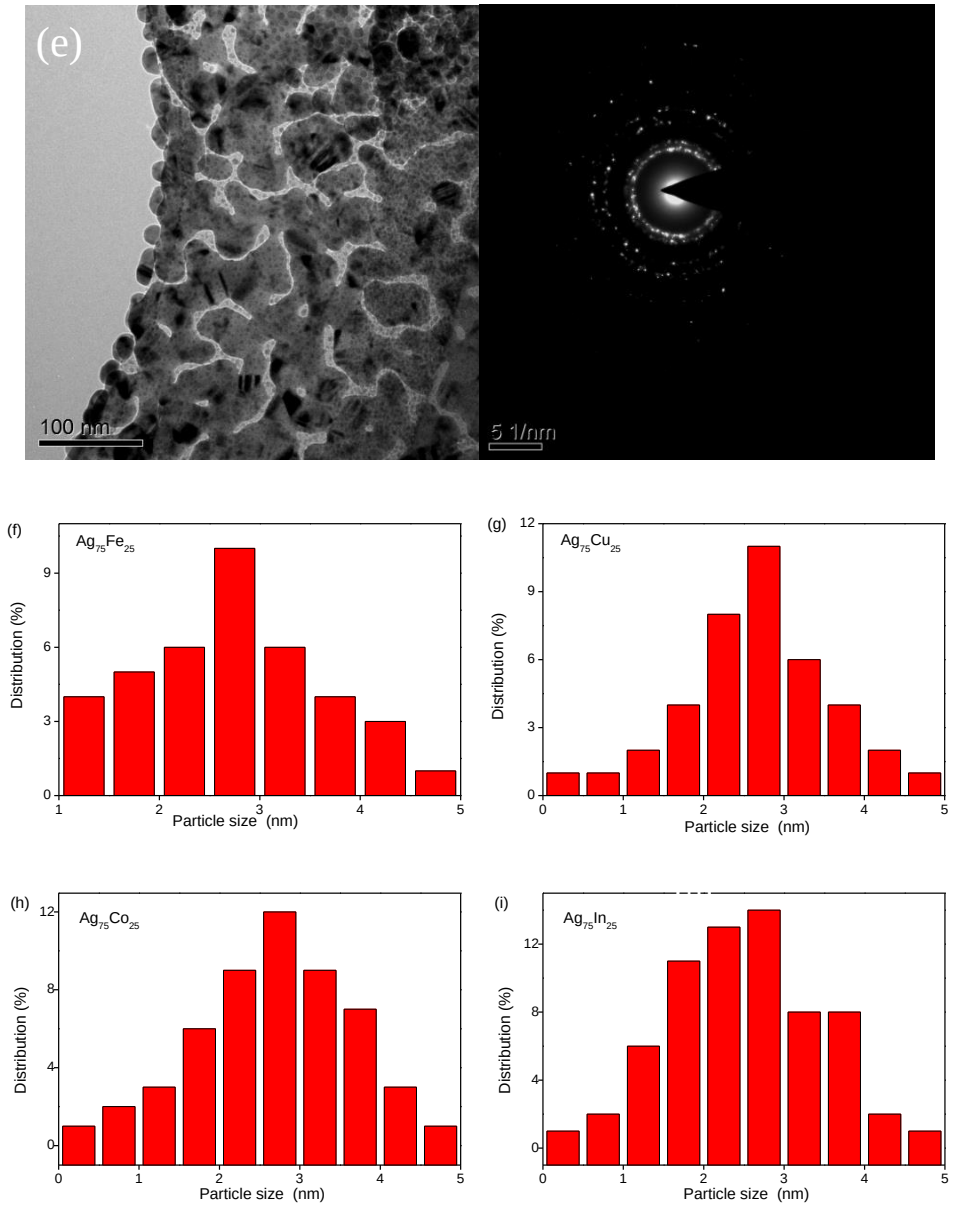

Figure S7. TEM images and selected area diffraction patterns (SAED) of the Ag-M alloys, (a) $Ag_{75}Fe_{25}$, (b) $Ag_{75}In_{25}$, (c) $Ag_{75}Co_{25}$, (d) $Ag_{50}Cu_{50}$, (e) Pure Ag, (f - i) particle size distribution of the Ag-M catalysts corresponding to TEM images.

Part 5. XPS results of Ag-M catalyst

Surface electronic structure properties

X-ray photoelectron spectroscopy (XPS) measurements were performed on an ULTRA (ESCALAB 250, Al Kα， ultrahigh vacuum is 10^{-9}， hν = 1486.6 eV). The data obtained is the typically of the samples. High-resolution O1s, Cu2p and Ag3d spectra were acquired. No charge compensation was necessary. The origin of the binding energy E_b was set to the Fermi energy E_f of the Au plate. The Shirley background is subtracted from the measured spectra. The d-band center of the valence band (VBS) is given by $\int R(\varepsilon)\varepsilon d\varepsilon / \int R(\varepsilon) d\varepsilon$, in this work, the R(ε) is the XPS-intensity (DOS-intensity) after background subtraction.[5]

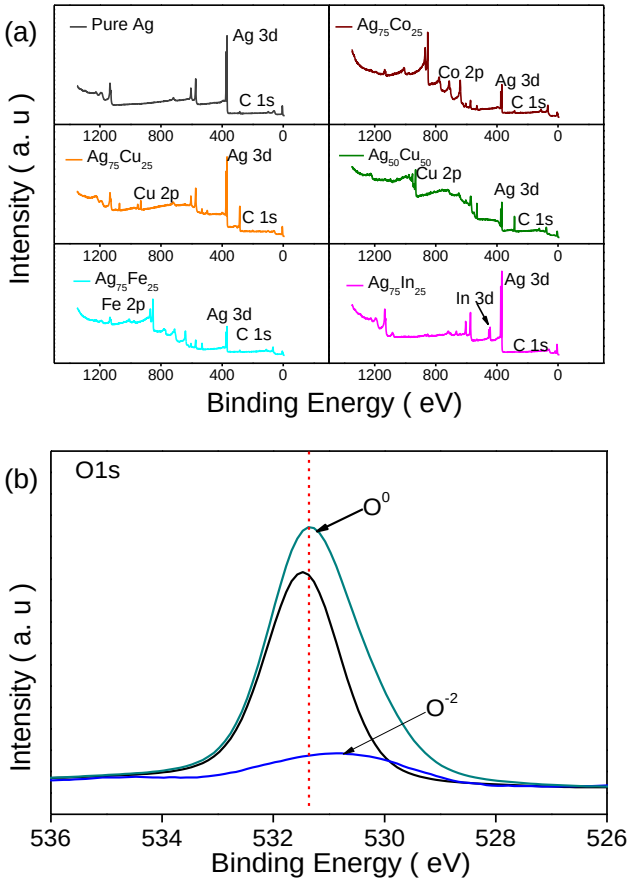

Figure S8. (a) Full survey scan XPS after Ar ion etching for the Ag, $Ag_{75}Co_{25}$, $Ag_{75}Cu_{25}$, $Ag_{50}Cu_{50}$, $Ag_{75}Fe_{25}$ and $Ag_{75}In_{25}$samples. (b) O_{1s} region in Ag-M alloys.

Part 6. Long-term stability analysis

Long-term stability of the $Ag_{75}Cu_{25}$ catalysts was assessed by accelerated testing, which was applied to the catalyst films in the same rotating disc electrode setup. The ORR curves at 1600 rpm, were recorded after 100, 600, 1000, 2000, 3000, 4000, 5000, 6000, 7000, 8000 and 9000 cycles. The Pb-stripping measurements was not performed at different cycle stage for one sample because we noted that the Pb- sripping measurements would pollute the catalyst surface, as shown in Figure S8c.[1] Hence, we prepared 14 different samples, in similar conditions, and performed the long-term stability test for each pattern in same way by measuring the ORR polarization curve of $Ag_{75}Cu_{25}$ alloys after different cycles.

Table S3. Comparisons of Pb-stripping area, surface charge and ECSA of $Ag_{75}Cu_{25}$ alloy after 100, 600, 1000, 2000, 3000, 4000, 5000, 6000, 7000, 8000 and 9000 cycles accelerated stability test.

Catalyst	Area of Pb-stripping (A)	Surface charge (Q_h)	ECSA	Change of ECSA relative to the first cycle *ΔECSA*
	$\int j(E)dE/V$	$\times 10^6$ uC/g_{Ag}	m^2/g_{Ag}	m^2/g_{Ag}
1	554.0	46.16	16.49	0
100	553.73	46.14	16.48	-0.01
600	551.38	45.95	16.41	-0.08
1000	547.94	45.66	16.30	-0.11
2000	541.02	45.09	16.10	-0.39
3000	535.84	44.65	15.95	-0.54
4000	527.50	43.96	15.70	-0.79
5000	520.07	43.34	15.47	-1.02
6000	511.68	42.64	15.22	-1.27
7000	505.81	42.15	15.05	-1.44
8000	493.94	41.16	14.70	-1.79
9000	478.42	39.87	14.24	-2.25

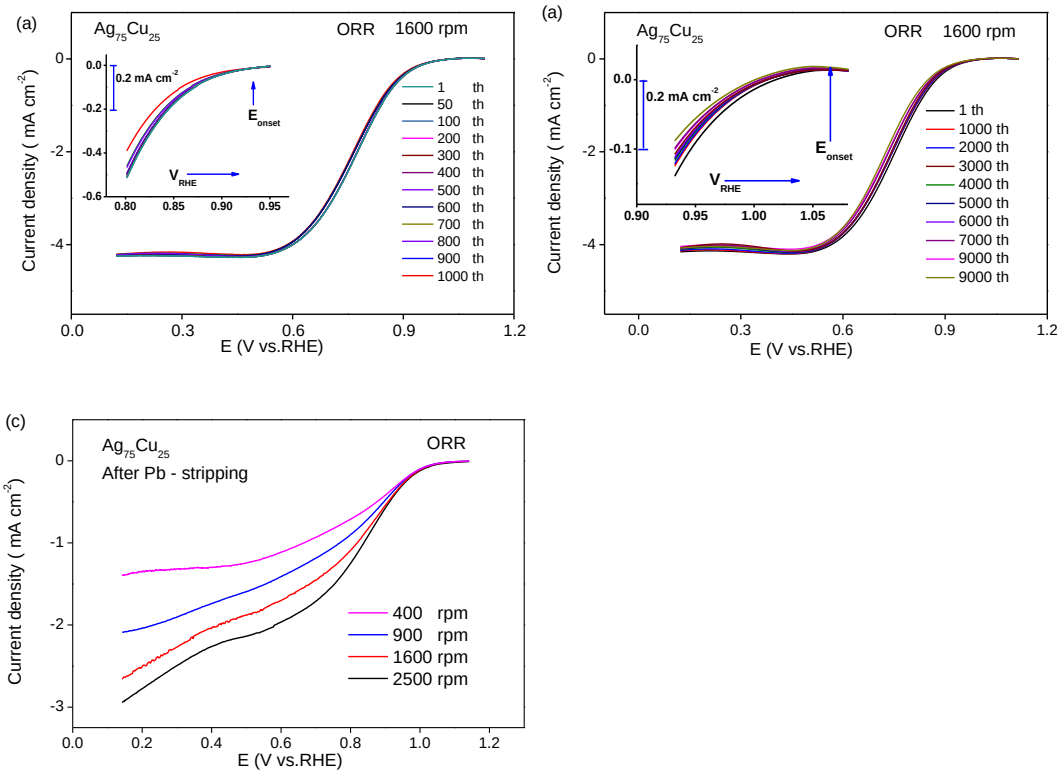

Figure S9. (a-b) The ORR polarization curves of $Ag_{75}Cu_{25}$ alloy after 100, 600, 1000, 2000, 3000, 4000, 5000, 6000, 7000, 8000 and 9000 cycles. (c) the ORR polarization curve of $Ag_{75}Cu_{25}$ alloy after Pb-stripping voltammetry test.

References

1. A. Holewinski; J.C. Idrobo; S. Linic, *Nat. Chem.* **2014**, *6*, 828-34.
2. a) F.J. Vidal-Iglesias; J. Solla-Gullon; V. Montiel; A. Aldaz, *Electrochem. Commun.***2012**, *15*, 42-45; b) J. Masa; C. Batchelor-McAuley; W. Schuhmann; R.G. Compton, *Nano Res.* **2014,** *7*, 71-78.
3. Y.Y. Liu; H.L. Jiang; Y.H. Zhu; X.L. Yang; C.Z. Li, *J. Mater. Chem. A* **2016**, *4*, 1694-1701.
4. E. Kirowa-Eisner; D. Tzur; E. Gileadi, *J.Electroanalyt. Chem.* **2008**, *621*, 146-158.
5. S.J. Hwang; S.K. Kim; J.G. Lee; S.C. Lee; J.H. Jang; P. Kim; T.H. Lim; Y.E. Sung; S.J. Yoo, *J. Am. Chem.l Soc.* **2012**, *134*, 19508-11.